REPORT DOCUMENTATION PAGE

1

Form Approved OMB NO. 0704-0188

1. REPORT DATE (DD-MM-YYYY)	2. REPORT TYPE	3. DATES COVERED (From - To)
22-09-2014	Final Report	1-May-2010 - 30-Apr-2014

4. TITLE AND SUBTITLE
Final Report: Rational Engineering of Reactive Nano-Laminates for Tunable Ignition and Power

5a. CONTRACT NUMBER
W911NF-10-1-0069

5b. GRANT NUMBER

5c. PROGRAM ELEMENT NUMBER
611102

6. AUTHORS
Jon-Paul Maria, Donald Brenner, Douglas Irving

5d. PROJECT NUMBER

5e. TASK NUMBER

5f. WORK UNIT NUMBER

7. PERFORMING ORGANIZATION NAMES AND ADDRESSES
North Carolina State University
2901 Sullivan Drive
Suite 240, Campus Bx 7514
Raleigh, NC 27695 -7003

8. PERFORMING ORGANIZATION REPORT NUMBER

9. SPONSORING/MONITORING AGENCY NAME(S) AND ADDRESS (ES)
U.S. Army Research Office
P.O. Box 12211
Research Triangle Park, NC 27709-2211

10. SPONSOR/MONITOR'S ACRONYM(S)
ARO

11. SPONSOR/MONITOR'S REPORT NUMBER(S)
57456-EG.2

12. DISTRIBUTION AVAILIBILITY STATEMENT
Approved for Public Release; Distribution Unlimited

13. SUPPLEMENTARY NOTES
The views, opinions and/or findings contained in this report are those of the author(s) and should not contrued as an official Department of the Army position, policy or decision, unless so designated by other documentation.

14. ABSTRACT
During the final program year, the NCSU team completed a surface science study exploring the virgin interfaces in reactive nanolaminates, completed a calorimetry study of three different thermite families, and initiated a Kirkendall-type experiment in Zr-CuO layered structure. Collectively, this learning completed the overarching program objective of predicting and tailoring the performance of nanolaminates using the material properties of the termial oxide phase. In addition, the team developed a modeling approach that can predict time dependent temperature profiles of electrically ignited thermite multilayers, and can predict/recreate differential scanning

15. SUBJECT TERMS
nanolaminate, thermite, thin film

16. SECURITY CLASSIFICATION OF:			17. LIMITATION OF ABSTRACT	15. NUMBER OF PAGES	19a. NAME OF RESPONSIBLE PERSON
a. REPORT	b. ABSTRACT	c. THIS PAGE			Jon-Paul Maria
UU	UU	UU	UU		19b. TELEPHONE NUMBER 919-522-9310

Report Title

Final Report: Rational Engineering of Reactive Nano-Laminates for Tunable Ignition and Power

ABSTRACT

During the final program year, the NCSU team completed a surface science study exploring the virgin interfaces in reactive nanolaminates, completed a calorimetry study of three different thermite families, and initiated a Kirkendall-type experiment in Zr-CuO layered structure. Collectively, this learning completed the overarching program objective of predicting and tailoring the performance of nanolaminates using the material properties of the termial oxide phase. In addition, the team developed a modeling approach that can predict time dependent temperature profiles of electrically ignited thermite multilayers, and can predict/recreate differential scanning calorimetry experiments.

Enter List of papers submitted or published that acknowledge ARO support from the start of the project to the date of this printing. List the papers, including journal references, in the following categories:

(a) Papers published in peer-reviewed journals (N/A for none)

Received		Paper
08/11/2014	1.00	Ed Mily, Andedapo Oni, James LeBeau, Yi Liu, Harlan Brown-Shaklee, Jon Ihlefeld, Jon-Paul Maria. The role of terminal oxide structure and properties in nanothermite reactions, Thin Solid Films, (07 2014): 405. doi: 10.1016/j.tsf.2014.05.005
TOTAL:	**1**	

Number of Papers published in peer-reviewed journals:

(b) Papers published in non-peer-reviewed journals (N/A for none)

Received		Paper
TOTAL:		

Number of Papers published in non peer-reviewed journals:

(c) Presentations

Annual Meeting of the American Vacuum Society 2014 Fall Meeting

New Trends in Research of Energetic Materials 2014 Meeting

Gordon Research Conference on Energetic Materials 2014

Number of Presentations: 3.00 3

Non Peer-Reviewed Conference Proceeding publications (other than abstracts):

Received Paper

TOTAL:

Number of Non Peer-Reviewed Conference Proceeding publications (other than abstracts):

Peer-Reviewed Conference Proceeding publications (other than abstracts):

Received Paper

TOTAL:

Number of Peer-Reviewed Conference Proceeding publications (other than abstracts):

(d) Manuscripts

Received Paper

TOTAL:

Number of Manuscripts:

Books

Received Book

TOTAL:

Received	Book Chapter

TOTAL:

Patents Submitted

Patents Awarded

Awards

Edward Mily was awarded 2nd place in the Best Oral Presentation competition in the 2014 NTRIM confernce in Pardubice Czech Republic

Graduate Students

NAME	PERCENT_SUPPORTED	Discipline
Ed Mily	1.00	
Xiaoyu Kang	0.33	
Shijing Liu	0.50	
FTE Equivalent:	**1.83**	
Total Number:	**3**	

Names of Post Doctorates

NAME	PERCENT_SUPPORTED
FTE Equivalent:	
Total Number:	

Names of Faculty Supported

NAME	PERCENT_SUPPORTED	National Academy Member
Jon-Paul Maria	0.08	
FTE Equivalent:	**0.08**	
Total Number:	**1**	

Names of Under Graduate students supported

NAME	PERCENT_SUPPORTED
FTE Equivalent:	
Total Number:	

Student Metrics

This section only applies to graduating undergraduates supported by this agreement in this reporting period

The number of undergraduates funded by this agreement who graduated during this period: 0.00

The number of undergraduates funded by this agreement who graduated during this period with a degree in science, mathematics, engineering, or technology fields:..... 0.00

The number of undergraduates funded by your agreement who graduated during this period and will continue to pursue a graduate or Ph.D. degree in science, mathematics, engineering, or technology fields:..... 0.00

Number of graduating undergraduates who achieved a 3.5 GPA to 4.0 (4.0 max scale):..... 0.00

Number of graduating undergraduates funded by a DoD funded Center of Excellence grant for Education, Research and Engineering:..... 0.00

The number of undergraduates funded by your agreement who graduated during this period and intend to work for the Department of Defense 0.00

The number of undergraduates funded by your agreement who graduated during this period and will receive scholarships or fellowships for further studies in science, mathematics, engineering or technology fields: 0.00

Names of Personnel receiving masters degrees

NAME

Total Number:

Names of personnel receiving PHDs

NAME

Total Number:

Names of other research staff

NAME	PERCENT_SUPPORTED

FTE Equivalent:

Total Number:

Sub Contractors (DD882)

Inventions (DD882)

Scientific Progress

This program year, the experimental component of our program completed two central experiments that complete the plan of work, initiated a new set of experiments that will be continued in a follow-on program, and initiated collaboration with two groups (Dlott - UIUC, and Zachariah - UMD) that perform advanced characterizations on reactive materials. This work is summarized below.

1. In situ Surface analysis
The NCSU group completed a sophisticated set of in situ xray photoelectron spectroscopy measurements where individual monolayers of metal were deposited on CuO surfaces with spectroscopic investigations of the surface, and the CuO metal interface on a layer-by-layer basis. These measurements were conducted for the Al-CuO and the Zr-CuO systems. We attempted to identify the intrinsic limits of interface formation that occur for these reactive systems.

For the Al-CuO case, we found that under very low energy conditions (materials prepared with ~kT energies, about 2 nm of Al2O3 forms at the Al-CuO interface, while for the Zr-CuO case, approximately 3 nm forms. What was most interesting to note is that small amounts of oxygen are scavenged from CuO in both cases, and that the amount scavenged depends strongly on time until full coverage of the CuO surface is complete. We believe that two pathways are possible for oxygen when the metal layer has yet to coalesce: 1) directly perpendicular to the metal/CuO interface, and 2) along the open CuO surface laterally to a metal hillock. This result is important because it indicates that the morphology of CuO surface, the deposition rate, and the wetting between CuO and metals will be very influential to determine how thin (and thus how much stored energy) and abrupt metal oxide / metal interfaces can be prepared and how reactive they can be.

2. Understanding mechanisms of thermite reaction
During the entire program, the NCSU team has been using calorimetry to determine the temperatures at which thermite nanolaminates reach the unstable exothermic condition as a function of layer thickness, substrate thermal mass, total layers present, diffusion coefficients, etc... To date, there has been debate regarding the mechanisms that occur at the very early stages, and which phases may be present and participating.

Most recently, the NCSU team identified a trend where the first exotherm appears to be associated with the eutectic temperature of an intermetallic composition between the reactive metal and copper metal, if that eutectic occurs below the temperature at which the nanolaminates would otherwise react by solid state means. In the Mg-CuO and Al-CuO systems, the first exotherms occur at temperatures corresponding to the lowest temperature eutectics in the Al-Cu and the Mg-Cu systems. This is important for two reasons: 1) it appears to explain the abrupt transitions observed in effective activation energy for laminates prepared with variable interface densities, and 2) it provides a completely new approach for engineering reactivity based on the phase equilibrium in intermetallic systems. We hypothesize at this point that with increasing interface density, there is an increase in the relative volume of eutectic liquid. When the volume reaches a critical value, the kinetics associated with a liquid phase take over, and an apparently lower effective activation energy are observed. Additional work pursuing this hypothesis are ongoing.

A summary of the modeling approach developed to simulate and understand DSC curves for reactive laminates is appended to this document. Appending as a PDF is necessary due to the substantial amount of equations.

Technology Transfer

none to report

REACTIVE NANOLAMINATES WITH TAILORED YIELD

PI: Prof. Jon-Paul Maria
Co-PIs: Prof. Donald Brenner and Prof. Douglas Irving
North Carolina State University
Department of Materials Science and Engineering

Program Manager: Ralph Anthenian Jr. PhD PE
Army Research Office,
Mechanical Sciences Division

FINAL PROGRAM REPORT

July 31, 2014

ABSTRACT

A combination of modeling and experimental synthesis were conducted top test our central program hypothesis: a mechanistic understanding of oxygen exchange at the nanoscale enables the rational design of metal / metal-oxide composites with tunable and predictable performance at the meso- and macro- scales. The outcomes will help enable a new class of energetic structures: (1) with theoretical energy densities significantly higher than conventional munitions (~3X RDX); (2) that can be less susceptible to accidental initiation via shock loading than conventional munitions; and (3) that present an opportunity for tunable ignition. Prototypical nano-laminates with nm-scale control were be fabricated using physical vapor deposition. Laminate components were selected using a new set of criteria based on the crystallochemical properties of the terminal as opposed to initial phases. This novel perspective enbled new material combinations and enhanced ability to regulate the energy release rates. In the companion theory and modeling studies, the Dynamics of Joule heating, reaction initiation, and self-sustaining reaction propagation were studies in a thermodynamic model that successfully predicts/simulates the calorimetric response of a virtual exothermic laminate reaction. In so doing, the models help to understand the mechanisms of transport during oxygen exchange.

Background: Nanocomposites that store energy via chemical segregation are of military importance as both energetic structural materials and as smart initiators. Their utility stems from exceptionally high energy densities, and ignition strategies with potentially tunable intensity. Harnessing these capabilities requires a fundamental understanding of the structure-property relationships that regulate mass transport during the spontaneous chemical reactions.

Our program focused on composites that release energy by oxygen exchange from a cation of higher electronegativity to a cation of lower electronegativity. Free energy minimization dictates the amount of energy released; however, the power output depends upon the kinetics of oxygen diffusion, thus the structural, thermal, and mechanical properties of the constituent phases. As such, our program will identify the material properties and engineering parameters that regulate transport and consequently identify options for tunable power release. This is a new approach that focuses on the properties of the terminal phases since these control mass transport during the majority of the

conversion reaction. We expect to identify alternative material combinations with enhanced capabilities using this novel approach.

This report is organized into 5 overarching experiments, each of which explores one or more aspects of the guiding hypotheses. The data given below summarize the most important finding in each category. The individual summaries are each an amalgam of multiple semesters of laboratory research. The experiments include:

1. Instrumentation upfit for multilayer fabrication
2. Validate high quality nanolaminate structure deposition
3. Demonstrate "slow" and "fast" nanolaminate design via crystal chemistry approach
4. Demonstrate the impact of layer thickness on laminate reaction initiation
5. XPS investigation of as-prepared interface reactions
6. Kissinger analysis of "slow" and "fast" oxygen exchange reactions
7. Computational approaches

EXPERIMENT 1: INSTRUMENTATION UPFIT

To ensure facile preparation of reactive nanolaminates, the NCSU team took an existing PVD system previously used to prepare ultrathin dielectric multilayers and converted it for reactive nanolaminate deposition. To do so, the system was cleaned internally, leak checked, and a second 2" diameter magnetron source was added. In addition, a shuttering mechanism to minimize cross-talk between the sources was engineered and installed. Figure 1 shows a schematic of the dual-magnetron PVD system. Two sources (nominally and oxygen source and an oxygen sink) are opposed at 180° incidence, each facing a

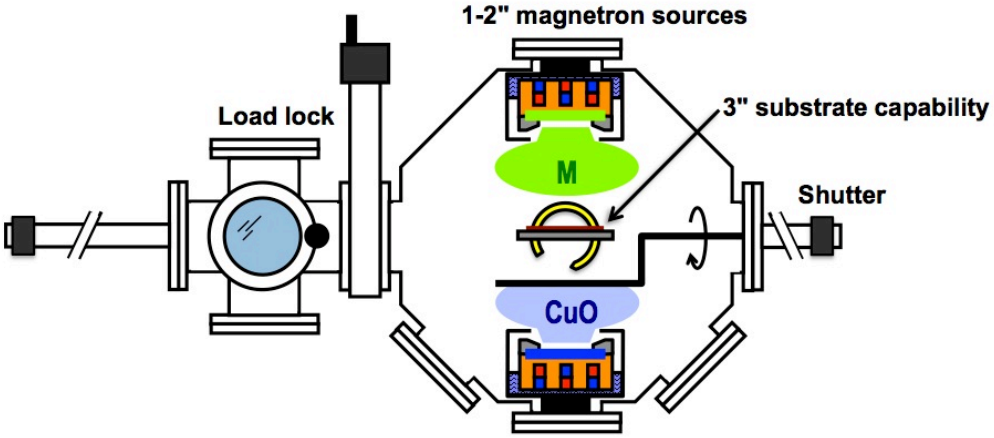

Figure 1: Schematic of NCSU dual-magnetron sputtering system optimized for naolaminate deposition

rotatable substrate manipulator, and each isolatable from its neighbor by a rotating shutter. Initial experiments with the instrument involved rate and uniformity calibrations, as well as assessments of purity of as deposited metal layers. To assess contamination, reactive metal films like Ti, Zr, and Al, were deposited in pure Ar. Their resistivity values were measured and compared to bulk data. If resistivities were 2X to 3X greater than the single crystal values, the system was considered clean. In all cases these criteria were satisfied.

EXPERIMENT 2: VALIDATE HIGH QUALITY NANOLAMINATE STRUCTURE PREPARATION

The next step in our process was to demonstrate a generic ability to prepare multilayer stacks of oxygen source and oxygen sink material with practically abrupt interfaces and excellent control of morphology and layer uniformity. To do so, our first system was CuO and Cr. This system was chosen given previous group experience with Cr metal deposition and because CuO was identified as the ideal oxygen source candidate material. Figure 2 shows a TEM cross section of a 19 layer stoichiometric stack. Stoichiometric refers to a thickness ratio that provides sufficient moles of O in CuO to fully oxidize all of the initial Cr layers to Cr_2O_3. The uniformity in thickness and microstructure from bottom to top is evident from this cross section.

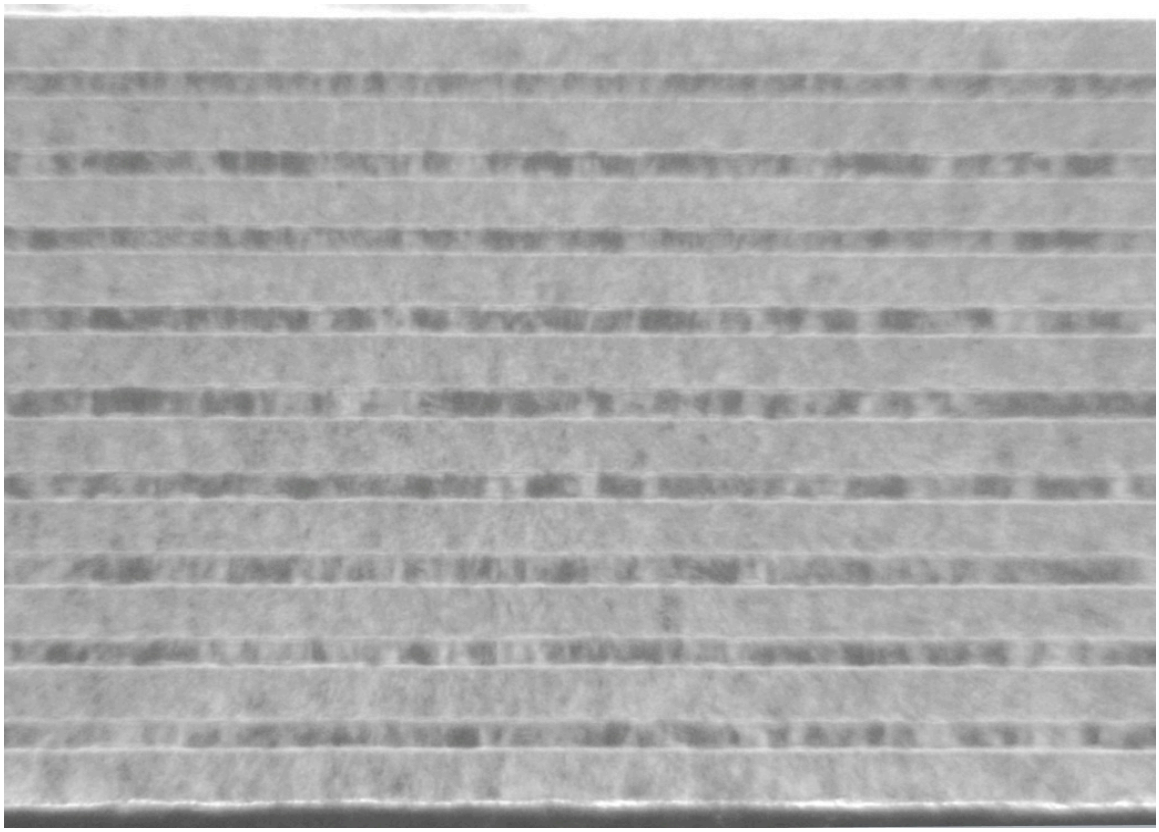

Figure 2: TEM cross section of CuO-Cr nanolaminate multilayer prepared in the NCSU dual-magnetron system. Note the uniformity in layer thickness and morphology in the 19 layer stack. In this case the Cr layers are 100 nm thick and the CuO layers are 230 nm thick.

The TEM analysis of Figure 2 shows microscopic uniformity, but little information about the metal|oxide as-deposited interface. Figure 3 shows a much higher magnification image a single interface near the sample center. The polycrystalline and fine-grained nature of this sample makes atomic resolution extremely challenging, however, from this image it is clear that the interface layers present (there has to be a finite layer where Cr is bonded to oxygen) is one the order of or less than 1 nm. As such, we can be confident that artifacts from as-depostied oxidation will not impart a predominant influence on energy release during oxygen exchange.

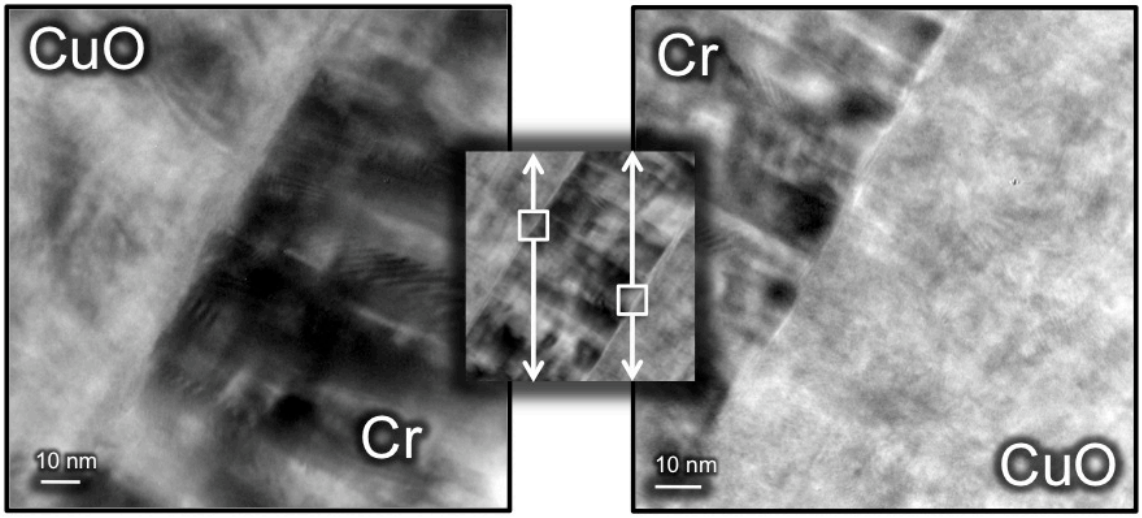

Figure 4: High magnification TEM image of as-deposited Cr|CuO interface showing that if present, as-deposited reaction layers are less than 1 nm.

The next step in our validation process was to determine if and when the oxygen exchange reaction could be initiated, how long it takes, and what are the terminal phase after reaction. To do so, a hot stage x-ray diffraction experiment was conducted for this CuO-Cr laminate. The data for this experiment, shown as a cascade of θ-2θ plots is shown in Figure 5.

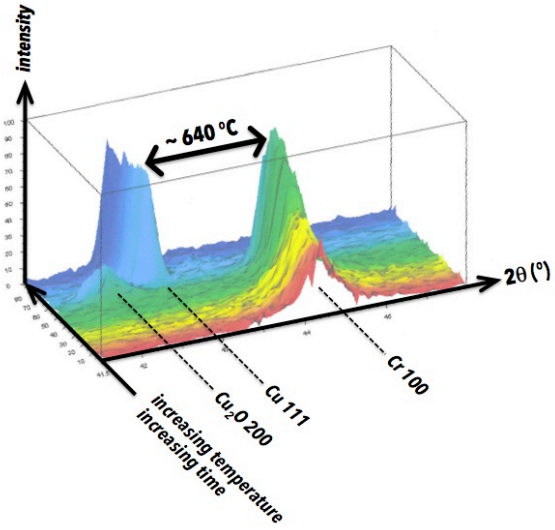

Figure 5: Schematic of NCSU dual-magnetron sputtering system optimized for naolaminate deposition

The data in Figure 5 show several important trends: 1) the initial oxygen exchange reaction occurs at temperatures around 640 °C; 2) the consumption of Cr is accompanied directly by the emergence of a strong Cu reflection; 3) the conversion occurs over ~ 10 °C window, and 4) during the conversion, a small peak corresponding to Cu_2O appears and is consumed. Collectively, these observations validate our ability to create as deposited nanolaminates that store chemical energy associated with oxygen exchange, which can be liberated by the addition of heat, which in principle provides the kinetic activity for oxygen exchange across the metal|oxide metastable interface.

EXPERIMENT 3: DEMONSTRATE "SLOW" AND "FAST" NANOLAMINATES

A central tenet of our activity was to explore the concept that the individual physical properties of the initial and terminal phases of a thermite-type reaction influence oxygen exchange more substantially than the free energies of oxidation associated with the conversion of initial to terminal oxide. We proposes an analogy to corrosion where the molar volume change that accompanies oxidation, the % covalency of the terminal oxide,

and the capacity of the terminal oxide to conduct oxygen determine exchange reaction rates. We believe that this set of material parameters is far more influential than thermodynamic minimization energies in determining kinetics and thus the rate of ignition. This hypothesis was tested using a set of experiments where one predicts and tests "fast" and "slow" nanolaminates whose material characteristics either promote or retard oxygen exchange.

Our initial experiment compared the properties of Cr|CuO and Zr|CuO laminates. To do so, stoichiometric laminates were prepared from each case with 19 layers. To the extent possible the laminates were of comparable total thickness. The thickness values could not be identical given the differences in density of Cr and Zr. To evaluate preliminarily the initial speed of reaction, the as-deposited laminates were inserted directly into a 800 °C tube furnace. The samples were imaged using either TEM or SEM both before and after heating. The results of each are shown in Figures 6 and 7.

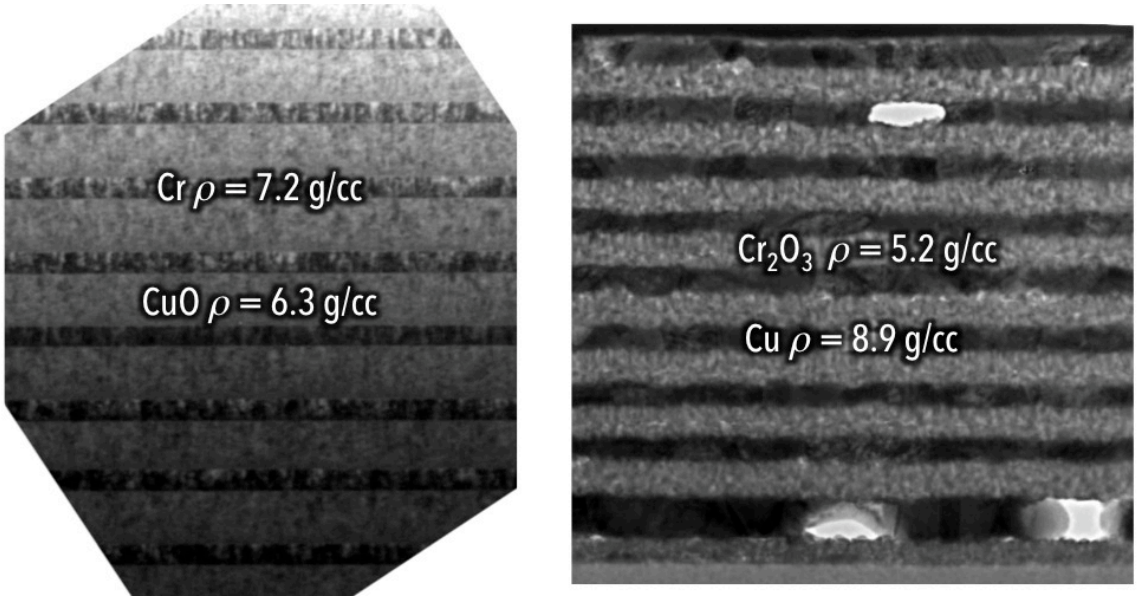

Figure 6: TEM analysis of a Cr|CuO nanolaminate structure before (left) and after (right) insertion into an 800 °C furnace

The TEM images of Figure 6 show a surprising result where the layering structure of Cu and Cr_2O_3 terminal phases are retained. This suggests a "gentle" oxygen exchange process where the overall laminate morphology was not lost. We speculate that this morphology can only occur when the oxygen exchange, and thus energy release, is slow. We expect this from Cr considering that oxygen diffusion through Cr_2O_3 is known to be very slow – consider that Cr is an important component of stainless steel where a Cr-rich surface oxide helps to prevent iron oxidation.

Alternatively, Figure 7 shows comparative images for the Zr|CuO laminate structure. The TEM image on the left shows uniform layering with sharp interfaces, while the SEM image on the right, taken after heating, shows a discontinuous microstructure with substantial substrate dewetting, with features that are reminiscent of rapid solidification. Such a surface microstructure is consistent with extremely high temperatures, which can only occur when stored chemical energy is released in a short time. Such temperatures would require rapid oxygen exchange. We expect this from A Zr-based laminate considering that oxygen diffusion through ZrO_2, the terminal oxide is one of the highest

values know for all oxides, and attributed to the cage-like unit cell of ZrO_2 with an open body center, and a propensity to accommodate oxygen deficiency.

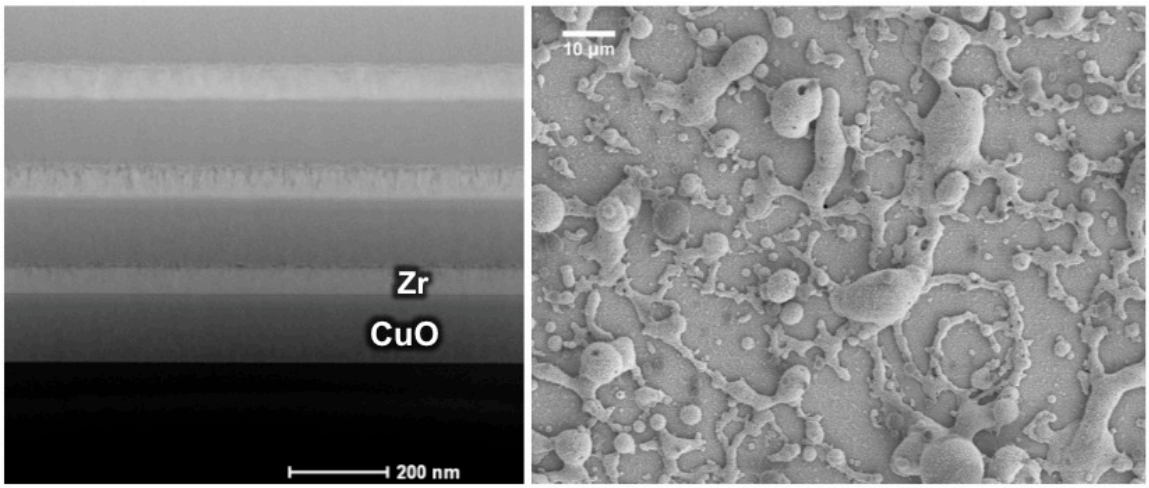

Figure 7: (left) TEM analysis of a Zr|CuO nanolaminate structure before and (right) SEM analysis of the Zr|CuO surface after insertion into an 800 °C furnace

To explore this concept in a less qualitative manner, a set of three laminates were selected based on the crystal-chemical aspects/properties of the terminal oxides. The selection of three enabled two direct property comparisons that would test the NCSU "corrosion" hypothesis. The three material comparison involved the following pairs:

- **Al-CuO and Zr-CuO:** Zr and Al represent extremes of oxygen conductivity. Al_2O_3 has a close packed anion sublattice thus no opportunities for anion conduction, while ZrO_2 features the fluorite structure that supports fast ion conduction.
- **Mg-CuO and Al-CuO:** Mg and Al are comparable with respect to their oxygen diffusion characteristics and their free energies of oxidation. However, while Mg and Al expand upon oxidation (+106% and +44% respectively), the expansion of MgO is substantially larger, which in principle leads to mechanical instabilities that promote mass transport.

The material properties of all three and a schematic of the samples prepared are compared in Figures 8 and 9 respectively. On a per mol oxygen basis, the oxidation of all three metals are comparable and at the upper end of oxidation energetics of all known metals. Consequently one expects a comparable driving force for scavenging oxygen with all three choices. When the diffusivity values are compared, the contrast is evident. At 500 °C, the speed at which oxygen can diffuse through the zirconia lattice is 15 to 20 orders of magnitude higher than for MgO and Al_2O_3 respectively. As mentioned above, the oxides of Mg and Al have comparable oxygen diffusion rates but their volume change upon oxidation are substantially different. The large expansion of MgO will likely cause instabilities that promote mass transport.

To experimentally test these hypotheses, nanolaminate stacks of each were prepared and heat treated. In this experiment, however, the samples were subjected to furnace anneals in argon (to avoid the influence of atmospheric oxygen) where the samples were again inserted to a pre-heated hot zone for 5 minutes and extracted. Sets of samples were heat treated over a ladder of temperatures from 300 °C to 800 °C in 100 °C increments.

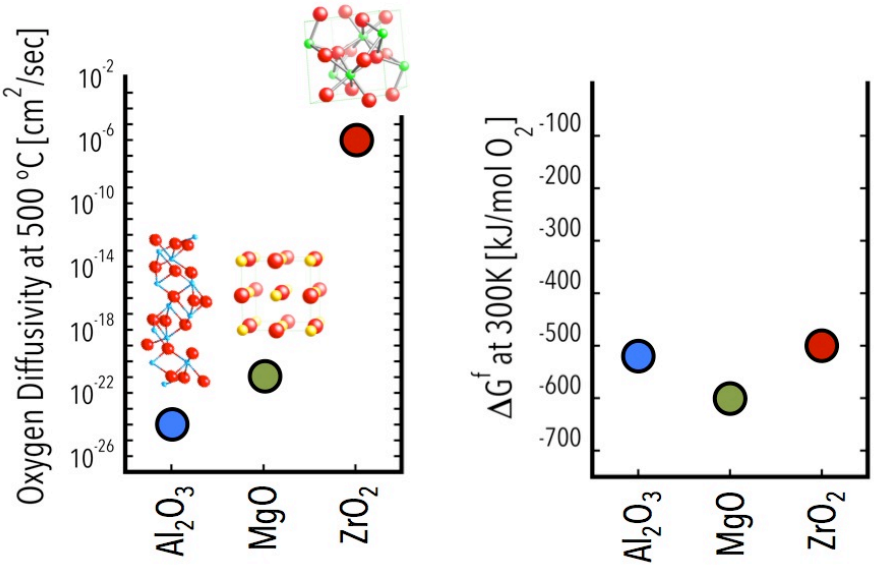

Figure 8: Property comparison of diffusivity and oxidation energy for the oxides of Al, Mg, and Zr

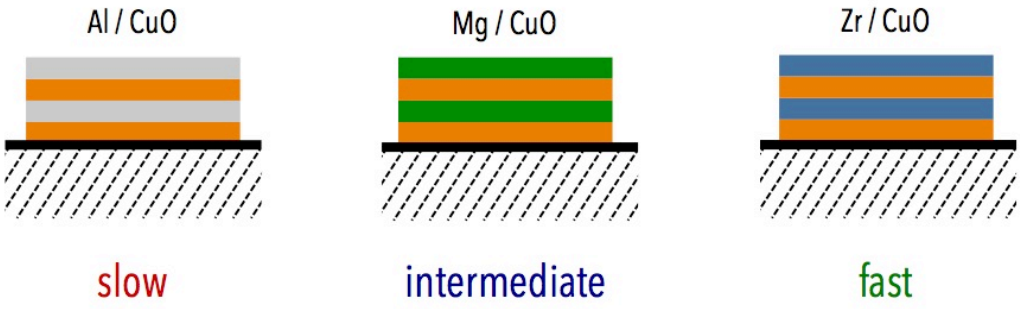

Figure 9: Schematic illustration of the three sample types tested in this comparison, and their proposed designation

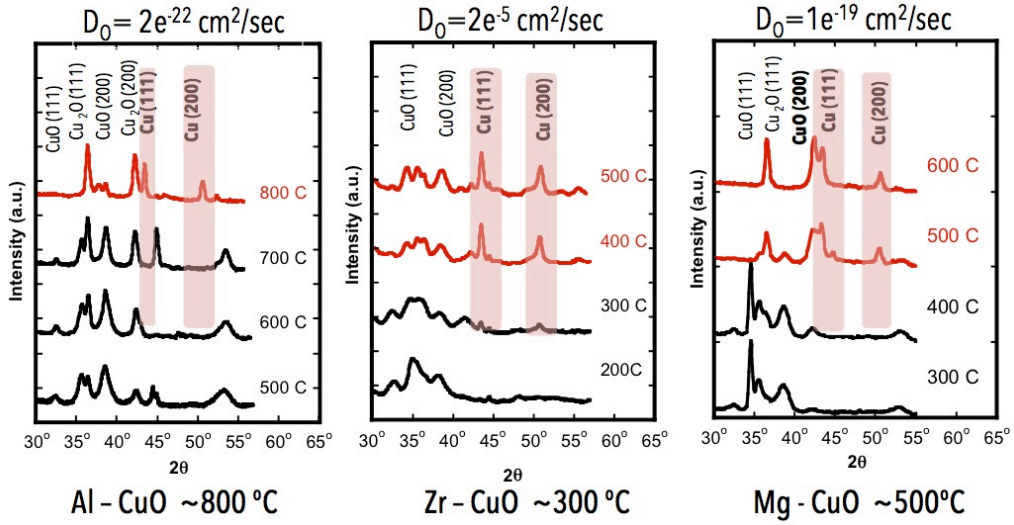

Figure 10: X-ray diffraction analysis for Al, Mg, and Zr-based nanolaminates as a function of thermal annealing in Ar

A summary of the x-ray data is shown in Figure 10. The left, middle, and right panels correspond to Al, Zr, and Mg-based multilayers respectively. Each graph includes x-ray spectra for each heat treatment temperature. The x-ray data was used to assess the temperature onset for reaction by noting the temperature at which the first sign of metallic copper was visible. Since a terminal product of the thermite reaction is Cu metal, it stands to reason that it's presence is a reasonable and self-consistent indicator that the oxygen exchange reaction is taking place. In each panel of Figure 10 the x-ray scans are color coded black and red, red meaning temperatures where Cu was detected. The onset temperature oxygen exchange reactions that produce Cu metal are 800 °C, 500 °C, and 300 °C for Al, Mg, and Zr respectively. This trend is consistent with our expectations regarding available mechanisms of mass transport, and it is reasonable to conclude that the terminal oxide properties are rather influential with respect to oxygen exchange.

As a final check, a 3 bilayer multilayer stack from each material system was evaluated upon heating in a differential scanning calorimeter (DSC). While quantification of calorimeter data is non-trivial, one can assess readily the onset of exothermic reactions. DSC traces for each system are shown in Figure 11.

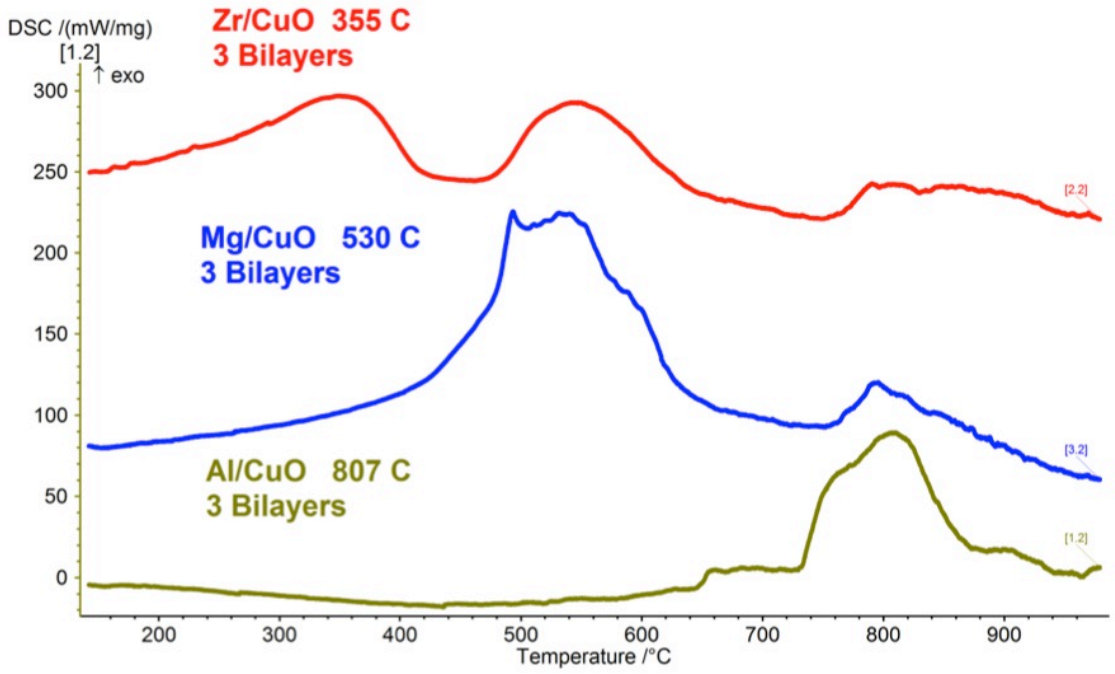

Figure 11: Differential scanning calorimetry traces for Zr, Mg, and Al-based nanolaminates. Each laminate has 3 metal|oxide bilayers in the as-prepared state. The heating rate was 5 °C/minute

We note in particular the temperature maxima of the first exotherm in each case: 350 °C, 530 °C, and 800 °C for Zr, Mg, and Al respectively. These data are again consistent with expectations from transport. It is important to note that these temperatures are nearly identical to those observed in x-ray diffraction for the onset of reaction. This is interesting because the heating rates in the furnace anneals and in the calorimeter are extremely different. For the case of Al, the sample was ramped for 160 minutes before reaching 800, while that same temperature is achieved in less than one minute when a sample is inserted into a pre-heated furnace. At this stage, the interpretation of this observation is speculative, the suggestion is that mass transport (within the rates explored

to date) is the limiting factor to reactions. That is to say, no matter how fast heat is added to the sample, cation or anion migration rates across the developing interfaces determine the temperature onset and extent of oxygen exchange.

EXPERIMENT 4: LAYER THICKNESS DEPENDENT OXYGEN EXCHANG REACTIONS

While our experiments to this point focused on the role of material properties in regulating oxygen exchange, it is clear that thermite-type reactions must also depend on physical boundary conditions. This dependence originates from the fact that self-sustaining reactions will always be governed by internal temperature, which is established ultimately by the relative rates of heat produced internally, and the rates at which heat is communicated to the surroundings.

To explore these dependencies, a series of experiments were conducted that changed the relative density of metal|metal-oxide interfaces in a film of constant volume. The illustration in Figure 12 shows the limiting cases of these sample geometries. Note in the figure that the total film thickness and thus the total volume of metal and metal oxide are constant. The only change is the density of interfaces.

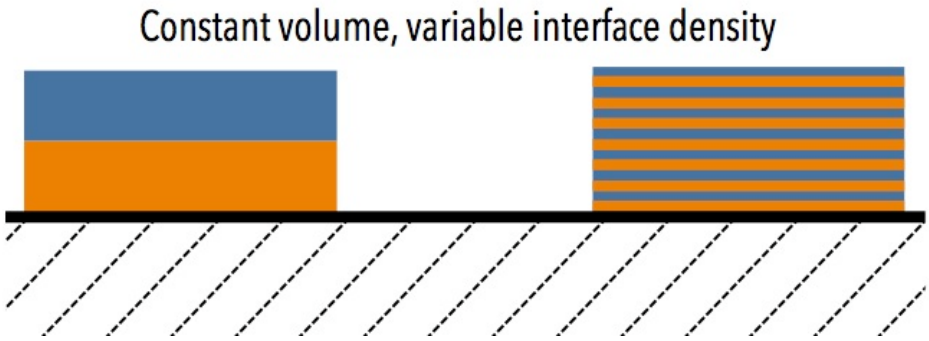

Figure 12: Schematic illustration of multilayer films used for experiments to determine the impact of interface density

A series of films with a total thickness on the order of one micron were prepared in the Zr|CuO and Al|CuO system. The number of bilayers was varied from 1 to 9 in the Zr system and from 1 to 13 in the Al system. If additional interfaces were added in either case, the layers became unstable, *i.e.*, the samples would spontaneously react when removed from the chamber, or sometimes during preparation.

The films were evaluated for onset of oxygen exchange reactions as in the previous experiment, i.e., each multilayer was heated for two minutes to a series of temperatures from 100 °C to 800 °C (the total range depended on the number of layers and the temperature of initial reaction). And an x-ray pattern was collected for each one. Again, thepresence of Cu metal in the post-annealed state was used to verify that the reaction started. Figure 13 shows the result for the Zr and Al-based systems at the maximum and minimum values for bilayer density. The x-ray patterns in red correspond to temperatures that produced Cu-metal.

The x-ray data show a clear trend where the apparent onset temperature for oxygen exchange reactions was lower for samples with higher interface densities. We explain this trend as follows: At the initial stages of reaction, all interfaces are indistinguishable, no

matter their density, and all have the same potential to produce heat. The furnace is the initial source of energy in all cases, and at some threshold temperature, there is sufficient heat to promote oxygen exchange across all interfaces. For a sample with one buried interface, the amount of area supporting the exothermic reaction is "A" for a sample with nine buried interfaces, the exothermic area is "9A". As such, with more buried interfaces, the energy density is much higher, so the internal sample temperature will be hotter for more interfaces given the same amount of heat from the environment. From these experiments, we conclude that the oxygen exchange reactions can be heavily influenced by geometry.

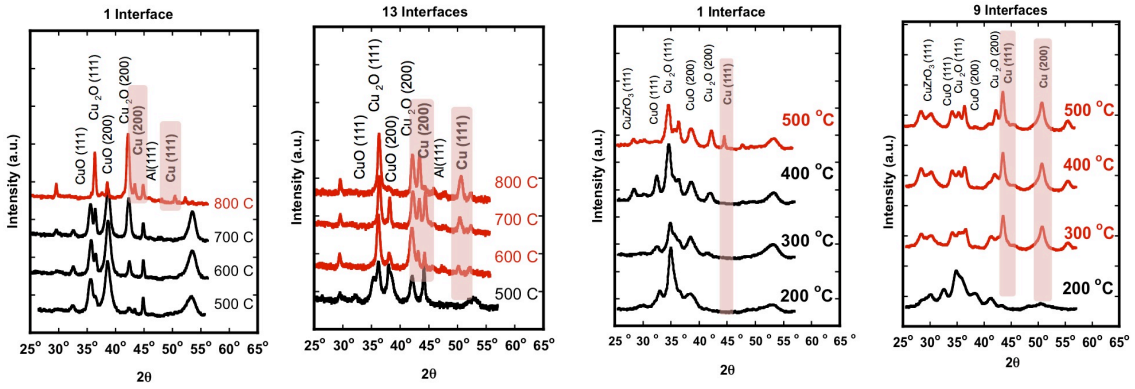

Figure 12: X-ray diffractin patterns for Al|CuO and Zr|CuO multilayers heated over a temperature ladder where the number of internal interfaces was varied while maintaining a constant sample thickness.

EXPERIMENT 5: KISSINGER ANALLYSIS OF AL|CUO AND ZR|CUO

To explore the geometric dependence further, the NCSU team performed a full Kissinger analysis where one collects calorimetric data as a function of heating rate to identify the functional relationship between an exothermic event and heating rate. In so doing, one can quantify activation energies (or at least effective activation energies) for these laminate systems. This analysis was conducted for the Al|CuO and Zr|CuO systems for each of the bilayer thicknesses explored in experiment 5: one through seven bilayers for Al|CuO and one through five bilayers for Zr|CuO. The raw DSC data showing exothermic events are shown in Figures 13 and 14.

In Figure 13, data for the Al|CuO system at a heating rate of 25 K/min, one finds a clear trend of decreasing temperature for the peak of the primary exotherm as the number of bilayers increases. This is consistent with the x-ray results of Figure 12 which showed the Cu-metal-producing reaction happening at lower temperatures for increasing bilayers, and is again consistent with the idea that these interface-dense samples produce heat at a faster rate. It is interesting to note that the general shapes of these curves changes at the 4-bilayer sample (this is true for all heating rates). While we do not, at this point, understand mechanistically what is happening, it is clear that for samples with a critical number of interfaces, there is a different mechanism occurring. Not only is there a discrete jump in temperature of the exotherm maximum, but the shape of the exotherm is distinctly different. The origin of this difference remains under investigation, but we speculate the participation of a liquid phase.

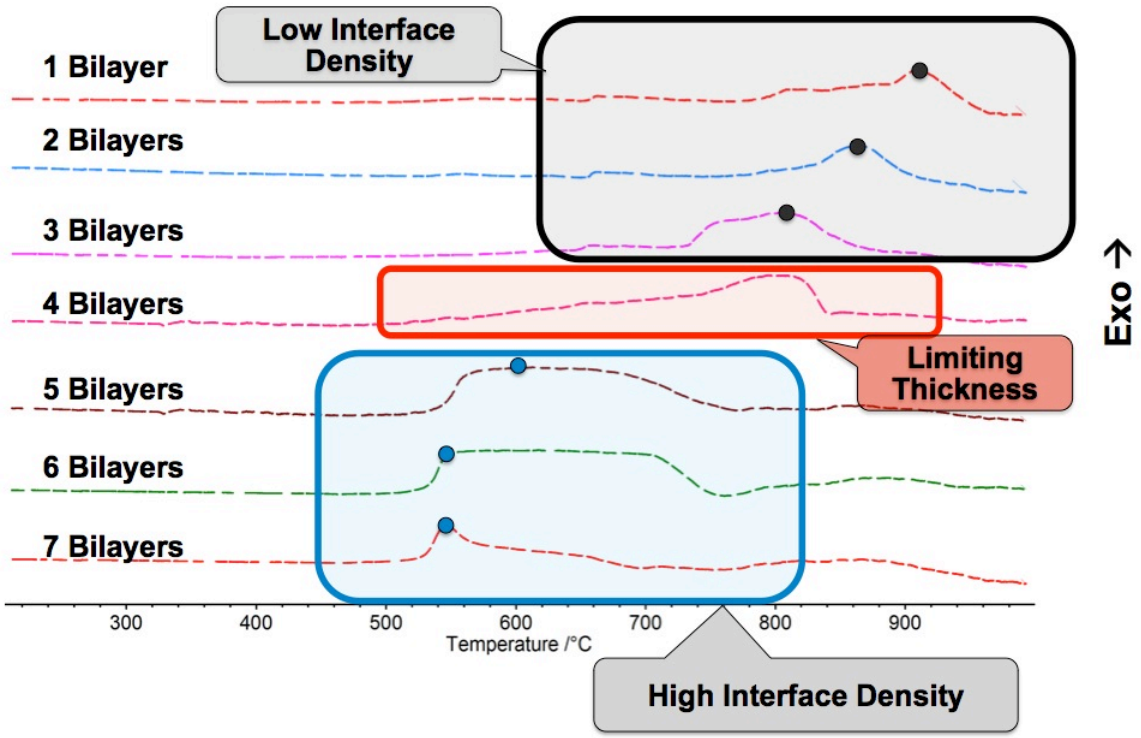

Figure 13: DSC curves for 25K/min heating rates for Al|CuO multilayers with variable interface density. All samples have identical total thickness. The blue dots indicate the temperature for the peak of the primary exotherm.

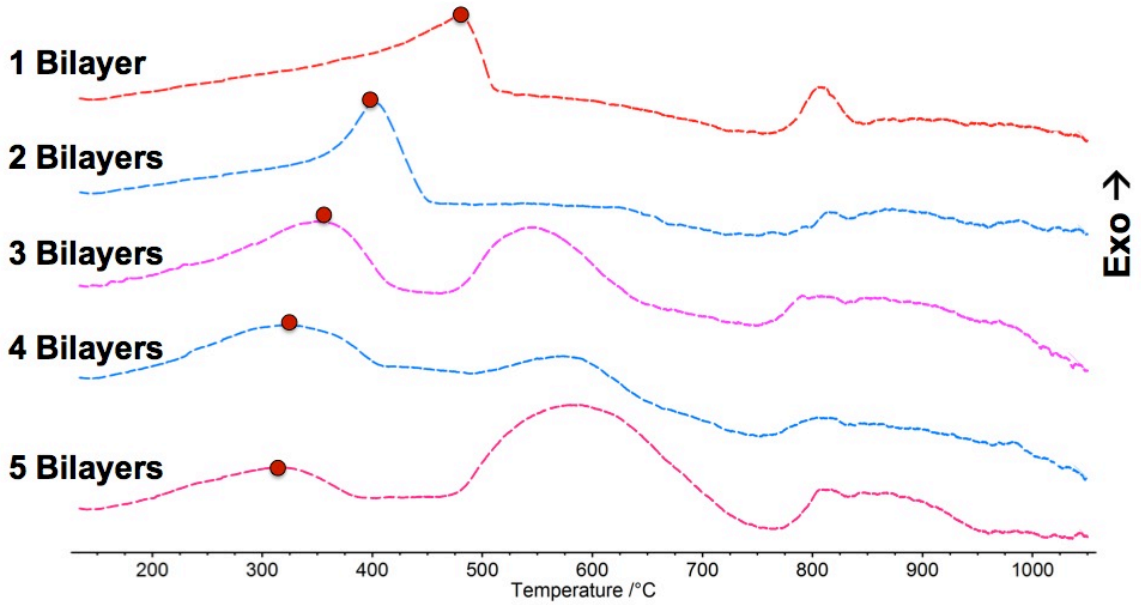

Figure 14: DSC curves for 25K/min heating rates for Zr|CuO multilayers with variable interface density. All samples have identical total thickness. The red dots indicate the temperature for the peak of the primary exotherm.

In Figure 14, data for the Zr|CuO system at a heating rate of 25 K/min, one again finds a clear trend of decreasing temperature for the peak of the primary exotherm as the number of bilayers increases. The trend, however, is distinctly different for the Zr-based system, there is no discrete jump in the peak exothermic event.

The entire data set for all heating rates (the slowest at 5K/min, the fastest at 25K/min) can be combined to complete the Kissinger analysis, which are plotted in Figure 15.

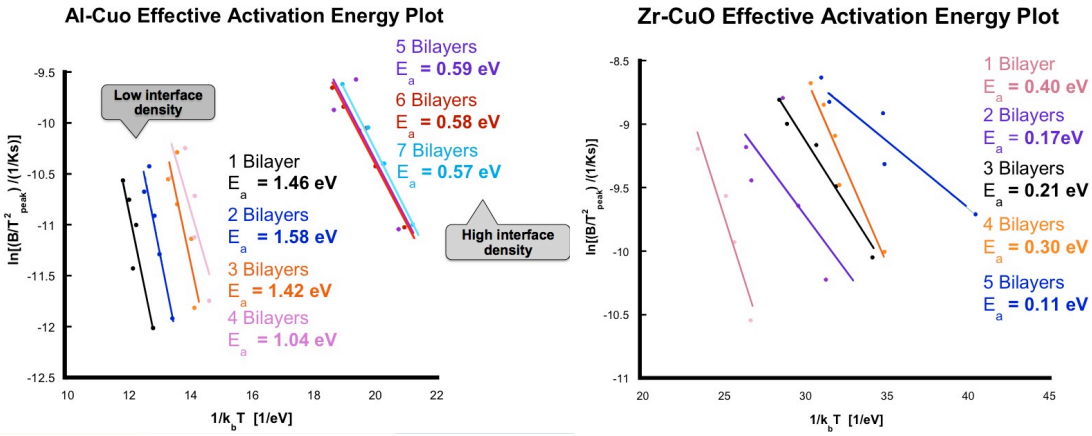

Figure 15: Kissiger analysis for the entire set of Al|CuO and Zr|CuO multilayers. Each data point corresponds to an average of multiple samples with a specific number of bilayers. The heating rates explored were 5, 10, 15, 20, and 25K/minute.

From the slopes of each curve one can extract an effective activation energy for the oxygen exchange process. In the Al-based system, the discrete jump in activation energies and the change in DSC shape corresponds to a substantial change in the effective activation energy. At this stage, the mechanisms for each are not clear, and remain under investigation. For the Zr-based system, a uniform activation energy is found for all layer thicknesses. While there appears to be substantially more scatter in the Zr-data, note that the magnitudes of the energies are substantially smaller.

While we cannot yet relate these activation energies to specific mechanisms of transport, Kissenger analysis remains a powerful method to compare the behavior of individual systems. Future comparisons with modeling efforts will help to make these connections.

EXPERIMENT 6: XPS ANALYSIS OF AS-DEPOSITED MATERIALS

To date, all of our experiments are conducted under the assumption that interfaces in the as-deposited state are abrupt and clean. In reality, we know that a finite quantity of unintentional oxide (of the reactive metal) must be present. In the extreme thin limit, the reactive metal is in contact with CuO, so there must be at least one metal-oxygen bond bridging the two materials. To explore these interfaces, we introduce a classic surface science approach where we prepare metal-oxide interfaces in ultra-high vacuum instruments where we can apply surface sensitive techniques to explore the interfacial evolution in situ. The specific instrumentation used is an x-ray photoelectron spectrometer that is connected to an e-beam evaporator via an ultra-high vacuum sample transfer tube. The vacuum in all chambers is sufficient such that during the entire

experiment, there is no impact/influence from the environment. Figure 16 shows a schematic of the UHV instrument that was used.

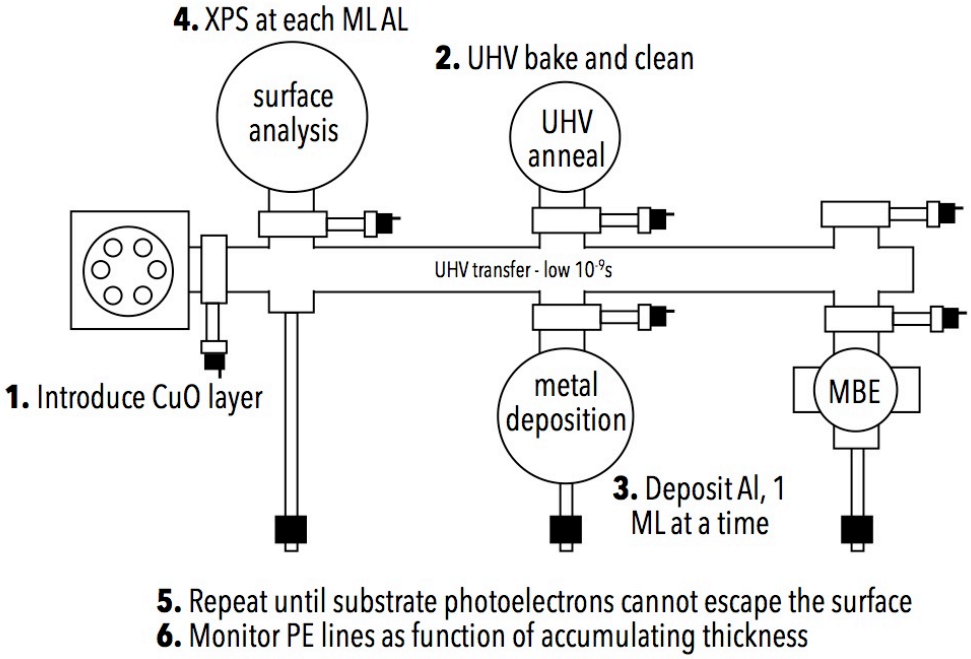

Figure 16: Schematic of UHV analysis, preparation, and deposition chamber used to characterize metal|CuO interfaces. The numbered sequence describes the process by which these interfaces are created and analyzed.

Two primary experiments were conducted, each following the same process. Initially, A CuO film was prepared on a Si substrate. The CuO film was introduced into the UHV annealing chamber to thermally desorb any water or organic material. That sample was transferred into the XPS chamber and spectroscopic analysis was conducted. After analysis, the samle was transferred into the e-beam deposition chamber and a specific number of monolayers of reactive metal were deposited. The sample was subsequently transferred back the the XPS system, where additional spectra were collected. For the Al and Zr systems, each metal thickness corresponds to an individual sample.

The initial question addressed corresponds to the Cu valence in the as prepared and coated scenario. Figure 17 shows a set of XPS spectra for a CuO film in the virgin state, and coated with 1 to 12 monolayers of Al metal. The energy range shown here corresponds to that containing the Cu photoelectron emission energies. In the as-sputtered state, the energies we observe correspond to those associtated with Cu with 2+ valence. In addition, we observe the broad CuO shake up lines near 940 eV which are associated with the CuO phase. From these data, we can conclude with confidence that our starting material is CuO. Note in this experiment, the data shown are for one sample, with spectra collected after each of 10 single-monolayer depositions.

As individual layers of Al are added, we observe peak shifts in the Cu photoelectrons to lower energies. These lower energy values correspond to a less-oxidized state, suggesting an environment more like Cu_2O. This is consistent with the reactive metal scavenging partially oxygen from CuO. With additional monolayers, we observe a constant Cu energy, but an attenuated peak. This occurs for two reasons: 1) there is more Al on the

film surface that absorbs and scatters the escaping electrons, and the CuO surface is becoming increasingly covered with Al. Note that for such low temperature depositions, growth occurs by first island formation, then subsequent coalescence.

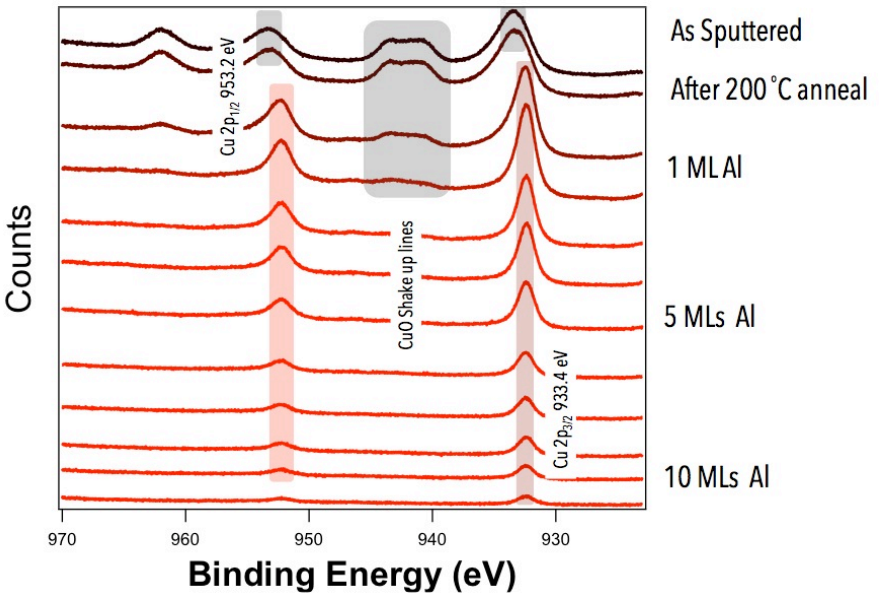

Figure 17: XPS analysis for a CuO surface coated with between 1 and 10 monolayers of Al metal. The energy range shown corresponds to that containing the Cu photoelectron energies.

The next experiment conducted explored the photoelectron energy ranges for the Al and Zr metal photoelectrons for CuO surfaces coated with various thicknesses of metal. Each spectrum corresponds to a different sample, i.e., the metal layers were deposited in one deposition. This was done to minimize the time between deposition and analysis. This is an important distinction because we know that these metal films are discontinuous until 5 to 10 monolayers are added. In the discontinuous state, lateral surface diffusion between the islands occurs over time and will obfuscate the information we seek. Fig. 18 shows the data for both metals.

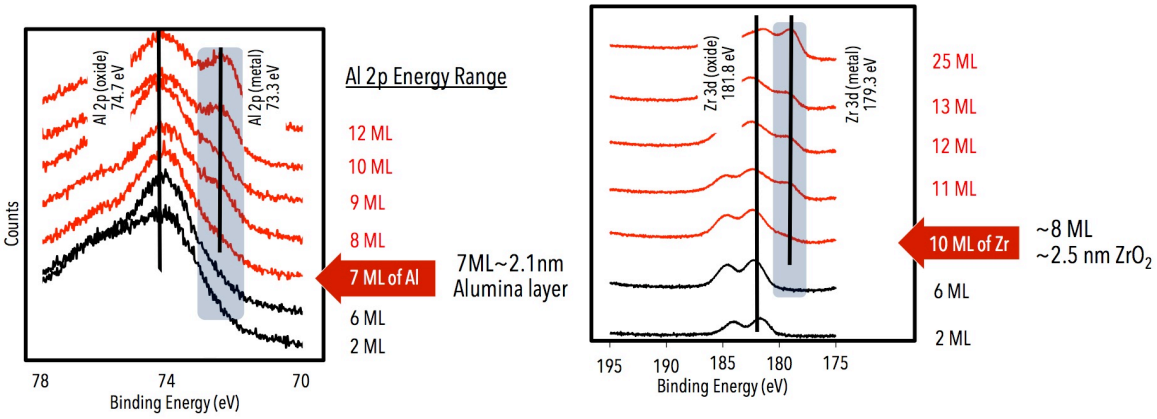

Figure 18: XPS analysis for Al and Zr depositions on a CuO surface collected for different deposited thicknesses. Each film thickness corresponds to an individual sample where the entire thickness was deposited at once. Two peaks are highlighted in each case, the peaks for the metallic and oxidized states.

In each case, there are two peaks highlighted, the peak associated with either Al or Zr in the metallic state, and the peak of either Al or Zr when coordinate (*i.e.*, bonded) to oxygen. The same trend is observed for each metal: for low numbers of monolayers, one only sees the metal oxide photoelectron line, which means that all of the deposited material scavenged oxygen from the CuO substrate. With increasing number of monolayers, a shoulder emerges in each, at an energy corresponding to the unoxidized metal. This occurs at ~7 and ~10 monolayers of Al and Zr respectively. The interpretation being that under these deposition conditions there is a transition layer between 2 and 3 nanometers thick for both systems.

It is interesting to note that the difference between Al and Zr is not particularly large, certainly not as large as the differences in oxygen transport properties between the oxide interface layers. This result suggests that the mechanisms during deposition, like surface mobility and wetting are likely to be substantial factors that influence the interface evolution, in addition to the thermodynamic propensity for oxidation.

EXPERIMENT 7: NUMERICAL CONTINUUM MODELING

A set of coupled partial different equations and associated numerical solver was developed to model nano-laminate reactivity at the continuum level. As detailed below, this modeling treats current transport and Joule heating, heat and mass transport, melting and chemical dynamics. The two examples described have significantly reduced the computational burden by mapping nano-laminate dynamics to two dimensions. Further studies will emphasize similar mappings where appropriate, as well as fully three-dimensional systems where needed.

Illustrated Figure 19 below are two example sets of numerical simulations, one that treats the X-Y cross sections and one that treats X-Z cross sections. The details and general results of the two simulations are presented below.

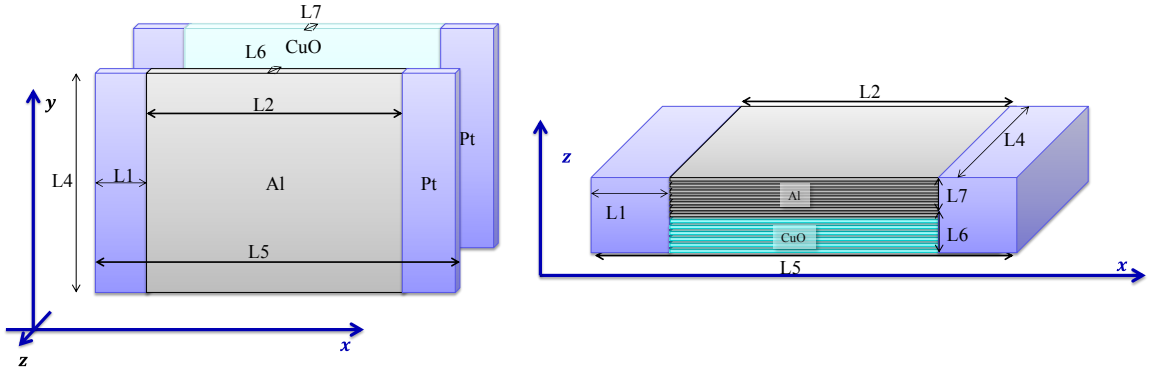

(a) (b)

Figure 19: Geometry of a Al-CuO multiple layer nano-laminate modeled by continuum dynamics. (a) Two separate two-dimensional planes with an Al film in the front and CuO foil in the back. The Z direction of each layer is thin and mapped into a two-dimensional model. (b) X-Y cross section where each mesh grid represents a mono-layer of either Al or CuO. The Y direction is homogeneous and mapped to a two-dimensional model.

SIMULATIONS ON INTERFACE PARALLEL PLANES

In this scheme, reactive models were restricted to two dimensional Cartesian coordinates. Two layers that correspond to metal and copper oxide were included in the system. Energy flow across the two layers is described by the heat conduction law

$$\dot{Q}_{T,C} = \kappa_{T,C}\Delta T \tag{1}$$

where $\dot{Q}_{T,C}$ is the heat conduction rate, $\kappa_{T,C}$ is the interfacial thermal conductance and ΔT is the temperature drop between the two layers. Other processes such as Joule heating, mass and heat transport (Fourier and Fick laws) chemical reactions and phase transformations (melting) are described by in-plane partial differential equations. For example, in-plane heat transport is assumed to follow Fourier's law:

$$\rho_m C_{p,m}\frac{\partial T}{\partial t} - \nabla\cdot(\kappa_T \nabla T) = \dot{Q}_{T,C} + \dot{Q}_r + \dot{Q}_m + \dot{Q}_e \tag{2}$$

where ρ_m is the mass density, $C_{p,m}$ is the specific heat capacity per unit mass, κ_T is the thermal conductivity, and $\dot{Q}_r$ is the heat generation rate from chemical reactions. The latter quantity has a positive value for exothermal reactions and a negative value for endothermic reactions. $\dot{Q}_m$ represents the heat change rates by phase transition, in our case, melting. $\dot{Q}_e$ is the heat generation rate due to joule heating which is described by:

$$\dot{Q}_e = \boldsymbol{J_e}\cdot\boldsymbol{E} = (\sigma_e \boldsymbol{E})\cdot(\boldsymbol{E}) = \sigma_e|\nabla\varphi_e|^2 \tag{3}$$

where $\boldsymbol{J}_e$ is the electric current density, $\boldsymbol{E}$ is the electric field strength, σ_e is the conductivity of the conductor and φ_e is the electric field potential. The conductivity is taken as a function of spatial coordinates and temperature as

$$\sigma_e = \frac{1}{\rho_e} = \frac{1}{\rho_{e0}[1+\alpha_{e0}(T-T_{e0})]} \tag{4}$$

where ρ_e is the electric resistivity of the conductor and ρ_{e0} is the resistivity at reference temperature T_{e0}. The parameter α_{e0} is an empirical parameter fitted from experimental data. According to Maxwell's equation, the electric potential field follows Laplace's equation

$$\nabla(-\sigma_e \nabla\varphi_e) = 0 \tag{5}$$

Thermite reactions are taken into account in different forms depending on the reaction stoichiometry. For example, the cupric thermite reaction with pure aluminum is

$$Al + 3/2\,CuO \rightarrow 1/2\,Al_2O_3 + 3/2\,Cu,\ \Delta G_f = 594.7\ \text{kJ/mol} \tag{6}$$

In our calculation, the extent of reaction is calculated from $f_{v,Al}$, which describes how much volume fraction of Al is been reacted. The heat generation rate from reaction can then be computed as

$$\dot{Q}_r = \dot{\xi}\cdot\Delta G_f = \frac{\rho_{m,Al}\dot{f}_{v,Al}}{M_{Al}}\Delta G_f \tag{7}$$

In addition, the reaction rate of Eq. (1) is assumed to follow an Arrhenius law:

$$\dot{\xi} = A\, e^{-\frac{E_a}{RT}} \tag{8}$$

where E_a and A are the activation energy and pre-exponential, respectively. Unless known from other sources, these are taken as parametric quantities in our modeling.

Similar to chemical reactions, melting of a substance α is described by $f_{l,\alpha}$, the fraction of liquid phase to total substance. In general

$$\tilde{\rho}_{m,\alpha} \Delta H_{m,\alpha}\, \dot{f}_{l,\alpha} = \dot{Q}_{m,\alpha} \tag{9}$$

where $\tilde{\rho}_{m,\alpha} \equiv f_{v,\alpha}\rho_{m,\alpha}$ and $\Delta H_{m,\alpha}$ are the effective mass density and the enthalpy change of melting of substance α, respectively.

Periodic boundary conditions for $y = 0$ and $y = L_4$ were used. Fixed boundary conditions for temperature and electric potential at $x = 0$ and $x = L_5$ were used, i.e.

$$\begin{aligned} &T|_{x=0} = T|_{x=L_5} = 0 \\ &\varphi|_{x=0} = 0, \qquad \varphi|_{x=L_5} = 0.1 \end{aligned} \tag{10}$$

Free surface boundary conditions for all other variables and other boundaries were used, e.g. $\left.\frac{\partial \varphi}{\partial x}\right|_{x=0,L_5} = 0$.

Equations (1) - (10) define a complete set of partial differential equations that are being investigated by numerical simulation.

SIMULATIONS OF PERPENDICULAR INTERFACE PLANES

Different from the first set of simulations, simulations on the XZ plane has allowed us to model mass and energy transport across alternative layers. This emphasizes the following aspects:

1. It is able to deal simultaneously with different mechanisms and further can be used to determine if (and where) there is a rate limiting step. For example, competition between oxygen and metal ion transport can be quantified;
2. Instead of only two layers, this simulation can model any arbitrary arrangement of the laminate structure. Therefore the factor of specific interface area can be taken into account.
3. In this configuration anisotropy is considered. More specifically, coordinates in the Z direction are discretized such that each grid point corresponds to one atomistic layer. This allows chemical reactions between atomistic layers to be treated differently from chemical reactions happening in the bulk. More Details are given in discussion of reaction (12) in the following.

Step functions of mole density of different substances are used to represent laminate structures. For example, $n_{Al}(x, z)$ describes how many moles of pure Aluminum per unit area is in the X-Z plane, i.e. the dimension of n_{Al} is mole/m^2. Furthermore, many processes are incorporated in this simulation. In addition to the general conservation law of mass and energy, those processes can be categorized into three groups.

(i) Chemical Reaction: Take cupric thermite reaction with pure aluminum as an example. It includes three elementary reactions, considered in Eq. (11), and two phenomenological reactions, as given in Eq. (12).

$$\begin{aligned} Al + 3/2\, O &\rightarrow 1/2\, Al_2O_3 \\ 2CuO &\rightleftharpoons Cu_2O + O \\ Cu_2O &\rightleftharpoons 2Cu + O \end{aligned} \tag{11}$$

$$\begin{aligned} Al + 3CuO &\rightarrow 1/2\, Al_2O_3 + 3/2\, Cu_2O \\ Al + 3/2\, Cu_2O &\rightarrow 1/2\, Al_2O_3 + 3Cu \end{aligned} \tag{12}$$

where the two direction harpoon symbol denotes reversible reactions while single direction refers to non-reversible reactions. Eq. (12) is not simply the linear combination of Eq. (11). This is because we assume that reaction (12) only happens between two atomistic layers through surface reconstruction other than ion transport as Eq. (11).

(ii) Ion transport: In this model all aluminum, copper and oxygen ions are considered as mobile. Flick's law is used to describe ion transport phenomenon with diffusivities taken from the Kakusan database [5].

(iii) Heat transfer and phase transformation: The same as in the other configuration, melting of all substances is considered. In contrast, however, anisotropic heat transfer is treated along the X and Z directions. This is because discretization along the Z direction is at the atom scale. Continuous thermal transport laws, such as Fourier's law, are no longer applicable. Instead we assume that energy flow across the atomistic layers follows the thermal conductance law as described in Eq. (1) and the thermal conductance is dependent on local composition of substances and temperature. Values are estimated from the online interfacial thermal conductance database (ITC) [6].

Each process corresponds to a phenomenological equation. However in general only two partial differential equations are solved in addition to the differential equations involving chemical reactions. The first one involves mass diffusion and balance

$$\frac{\partial n_\alpha}{\partial t} = \nabla \cdot (D_\alpha \nabla n_\alpha) + \sum_i \dot{n}_{\alpha,R_i} \tag{13}$$

where $\alpha = Al, Cu, Cu_2O, \ldots$ refers to different substances and $\dot{n}_{\alpha,R_i}$ refers to the change in the number of atoms of substance α due to reaction R_i. Similar to the mass transport equation, the energy equations is

$$n_\alpha C_{p,n} \frac{\partial T}{\partial t} = \nabla \cdot (\kappa_T \nabla T) + \dot{Q}_{R_i} \tag{14}$$

where $C_{p,n}$ is the standard specific heat (per unit mole) and $\dot{Q}_{R_i}$ is the heat released/consumed during chemical reaction R_i.

Chemical reactions can be described by ordinary differential equations whose forms are dependent on the order of the chemical reactions. Take the first reaction in Eq. (11) as an example; its governing equation is

$$\dot{n}_{Al,R(11)} = k_{R(11)}[O]$$
$$\dot{Q}_{Al,R(11)} = \dot{n}_{Al,R(11)} \times \Delta G_{R(11)} \quad (15)$$

where $[O]$ is the atom fraction of oxygen ion and ΔG_{R_i} is the standard free energy change.

Plotted in the Figure 20 are calculated temperature profiles from simulations of the first configuration discussed above. The two levels in panel (a) correspond to Al (top level) and copper oxide layers. At 0.001s after the voltage is applied the platinum leads heat quicker than both laminate layers, while the aluminum layer heats quicker than the copper oxide due to the higher resistivity of the latter. At time 0.025 s (panel (b)) both laminate structures have the same temperature due to heat transfer that approaches the metal leads. Plotted in panel (c) are the temperature profiles at 0.027 s, which is after initiation of the thermite reaction. At this applied voltage initiation of the thermite reaction occurs near the region where the thermite and lead meet. This results in extreme transient temperatures as apparent in panel (c).

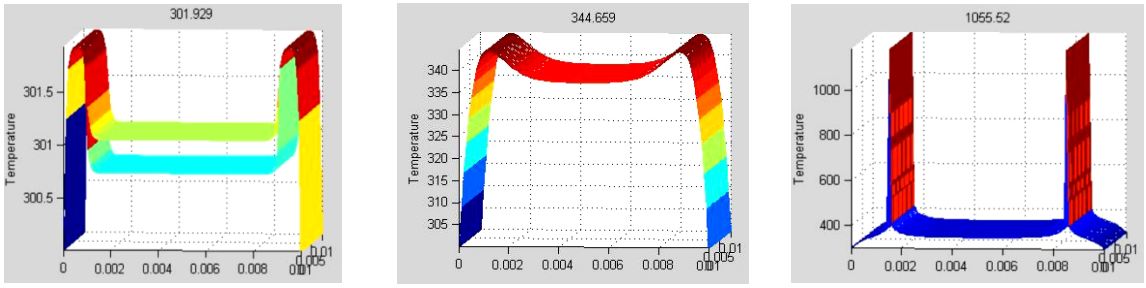

(a) (b) (c)

Figure 20: Temperature profiles that demonstrates the different stages during joule heating abd thermite reaction. (a) t=0.001s. (b) t=0.025s. (c) t=0.027s. The small time and large temperature difference between panels (b) and (c) compared to those between panels (a) and (b) is consistent with the delay time and rapid reaction observed experimentally

Plotted in Figure 21 below is the time before the rapid rise (thermite initiation) in the simulation as a function of the pre-factor in the reaction Arrhenius rate for constant activation energy of 150kJ/mole and an applied voltage of 0.1 eV. Smaller prefactors require longer times and hence more Joule before the self-sustaining reaction is initiated. From an analysis of this numerical data it appears the dependence of the time to initiation on the prefactor is a power law. Further theoretical analysis of this relationship is underway.

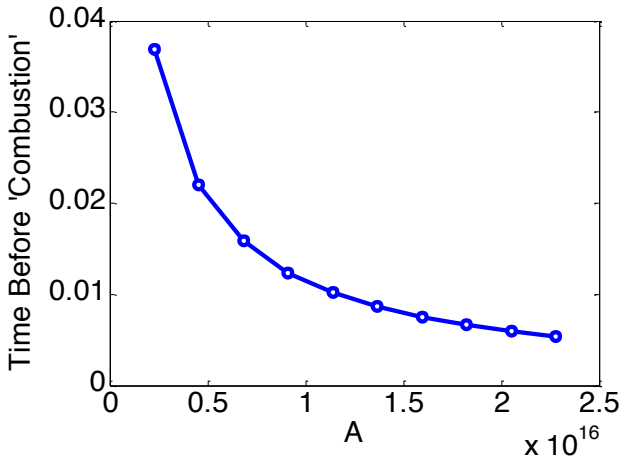

Figure 21: Time before initiation vs. pre-exponential component with Ea=150kJ/mol and applied potential V_1=0.1 V..

In traditional thermite modeling kinetic parameters such as activation energy and pre-exponent factor of the rate determining step is determined by comparing calculated reaction propagation speed to experiment values [7,8]. In our simulation, we found that reaction propagation speed is relatively independent of the pre exponent factor, but strongly correlated to activation energy as shown in Figures 22 and 23. This result is similar to the relationship of combustion wave speed and activation energy in metal powder combustion experiments [7,8].

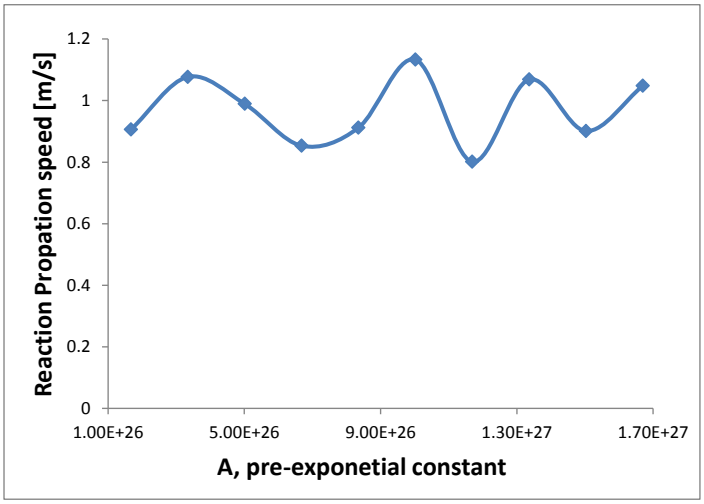

Figure 22: Dependence of reaction propagation speed on pre-exponential constant of Eq. (6).

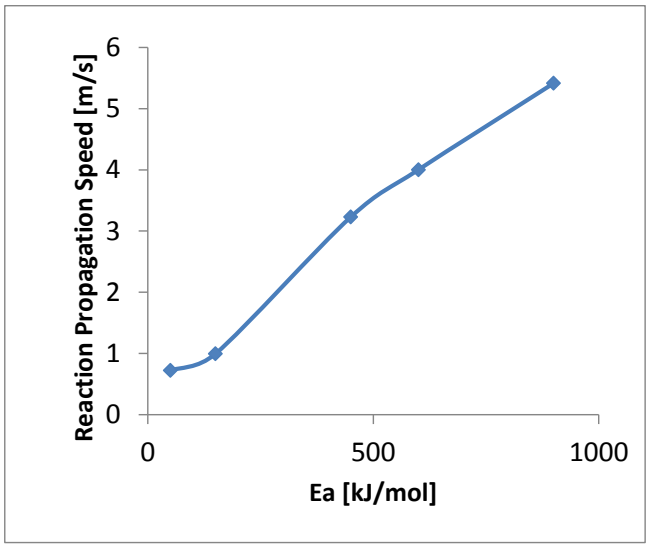

Fig. 23: Dependence of reaction propagation speed on activation energy of Eq. (6).

REFERENCES

[1]. J. E. Lewis and R. C. Plumb, JOURNAL OF THE ELECTROCHEMICAL SOCIETY, 105, 496 (1958).
[2]. G. Amsel and D. Samuel, J. Phys. Chem. Solids, 23, 1707 (19.62).
[3]. J. A. Davies, J. P. S. Pringle, R. L. Graham, and F. Brown, OURNAL OF THE ELECTROCHEMICAL SOCIETY, 109, 999 (1962).
[4]. Fan, H. J., Gösele, U., & Zacharias, M. (2007). Formation of nanotubes and hollow nanoparticles based on Kirkendall and diffusion processes: a review. Small (Weinheim an der Bergstrasse, Germany), 3(10), 1660–71. doi:10.1002/smll.200700382
[5] Diffusion Database (Kakusan). http://diffusion.nims.go.jp/index_en.html
[6] NIMS Interfacial thermal conductance database. http://interface.nims.go.jp/index_en.html
[7] Arimondi, M., Anselmi-Tamburini, U., Gobetti, A., Munir, Z. A., & Spinolo, G. (1997). Chemical Mechanism of the Zr + O 2 → ZrO 2 Combustion Synthesis Reaction. The Journal of Physical Chemistry B, 101(41), 8059–8068. doi:10.1021/jp963932r
[8] Maglia, F., Anselmi-Tamburini, U., Gennari, S., & Spinolo, G. (2001). Dynamic behaviour and chemical mechanism in the self-propagating high-temperature reaction between Zr powders and oxygen gas. Physical Chemistry Chemical Physics, 3(3), 489–496. doi:10.1039/b005678m